INVESTIGATION OF CONTACT FORMATION ON LOCALLY LASER-DOPED SURFACES ON A MICROSCOPIC SCALE

Daniel Wurmbrand, Heiko Plagwitz, Frank Huster, Giso Hahn, Barbara Terheiden
University of Konstanz, Department of Physics, 78457 Konstanz, Germany
Daniel.Wurmbrand@uni-konstanz.de Tel: +49 7531 885295

ABSTRACT: In this work we present a detailed investigation of the contact formation of screen-printed silver paste on locally laser-doped silicon surfaces by Kelvin probe force microscopy (KPFM) and scanning electron microscopy (SEM). Although laser doping has been studied many times in the past, there is a lack of systematic studies that shed light on the correlation of laser-induced surface modifications and the associated electrical contactability of the surface, on a microscopic scale. The use of phosphosilicate glass (PSG) deposited by atmospheric pressure chemical vapor deposition (APCVD) as a dopant source and a nanosecond pulsed laser, which can be operated with both a Gaussian and a flat-top beam profile, enables the generation of locally doped structures. Contacting by means of screen-printed silver paste and subsequent evaluation by transfer length method (TLM) shows that, depending on the selected laser parameters and pulse overlap, specific contact resistances can be obtained that vary by more than an order of magnitude. By using the aforementioned KPFM and SEM analysis methods, we show that laser pulse overlap is a key aspect affecting the extent of laser induced surface damage and ultimately silver crystallite growth.
Keywords: Laser doping, local doping, contact formation, APCVD

1 INTRODUCTION

Laser doping is with more than 80% the main process to create selective emitters in PERC (Passivated Emitter and Rear Cell) solar cells which are in turn the main cell product with above 80% in 2022 [1]. A sound overview on laser doping in its different aspects is given by Vaqueiro-Contreras et al. [2]. Vaqueiro-Contreras et al. showed that laser doping can be implemented besides in PERC also in PERT (Passivated Emitter and Rear Totally diffused) and TOPCon (Tunnel Oxide Passivated Contact) solar cell concepts [2].

In contrast to selective emitters, the application of laser doping for the generation of only locally doped areas has only rarely been investigated. Heilig et al. studied the different doping profiles from dopant containing silicate glasses that were used first as a dopant source and then treated locally with a laser, as is the common procedure to generate selective emitters, with dopant concentrations from “fresh” P containing silicate glasses (PSG, BSG) [3]. They also studied the difference of doping from $POCl_3$ formed PSG to PSG from APCVD (atmospheric pressure chemical vapor deposition). Using APCVD for PSG formation allows to create the desired locally laser doped areas, this is not possible with $POCl_3$ based PSG.

In this laser doping process, the laser radiation is transmitted almost unhindered by the dopant containing glass layer and absorbed near the surface in the silicon. In the area hit by the laser pulse, the silicon is melted which leads to local heating of the overlying glass layer. Liquid phase diffusion of the released dopant atoms takes place in the liquefied silicon. Finally, the molten silicon solidifies with the dopant atoms embedded. Since this process takes place on the nanosecond scale, defect formation during recrystallization of the silicon surface cannot be completely avoided under certain conditions [4]. Other studies investigated laser damage regarding the damage to the pyramid textured wafer surface and its effects on the efficiency of selective emitter solar cells [5].

The microscopic Ag contact formation on these laser-doped areas was not investigated up to now. Therefore, a systematic microscopic investigation by Kelvin probe force microscopy (KPFM) and scanning electron microscopy (SEM) of locally laser-doped surfaces with focus on Ag crystallite growth in dependence of laser process parameters is presented and related to specific contact resistivities ρ_C determined by the transfer length method (TLM).

2 EXPERIMENTAL

Figure *1* shows the process flow of sample preparation and subsequent analysis method. Different silicon substrates were used according to the different characterization methods. Low resistivity n-/p-type Czochralski (Cz) Si substrate (0.8 & 1.0 Ωcm, respectively) were textured using an aqueous alkaline etch solution based on KOH with alcohol-based additives.

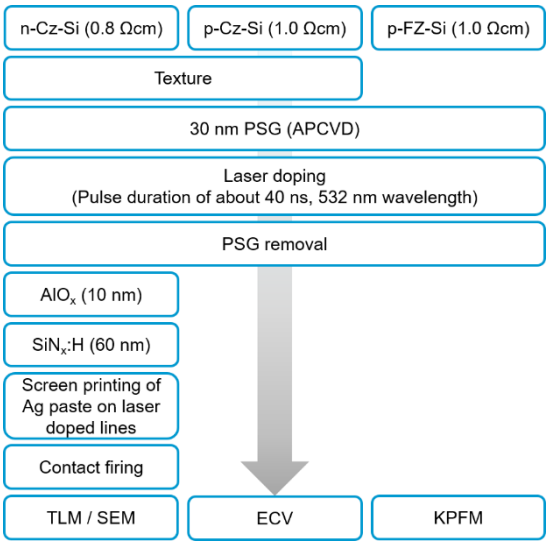

Figure 1: Process flow diagram of sample preparation

For the KPFM samples p-type float-zone (FZ) silicon substrates (1.0 Ωcm) have been used without alkaline texture to avoid roughness-related effects on the measurement of the surface potential. All samples receive a deposition of 30 nm PSG with a phosphorus content of about 8.0-8.5 at% by APCVD. For laser doping a pulsed

nanosecond laser (532 nm wavelength, ca. 40 ns pulse duration) with gaussian (G) or flat top (FT) pulse profile is used to create 120 µm wide laser doped lines (TLM and KPFM samples) or 2 x 2 cm^2 fields with full-area doping to determine doping profiles by electrochemical capacitance-voltage measurements (ECV). The remaining PSG layer and residues from the laser process were removed in diluted HF. Samples for TLM examination receive a typical passivation layer stack consisting of 10 nm AlO_x (APCVD) and 60 nm SiN_x:H (PECVD). 40 µm wide silver contacts are screen-printed onto the 120 µm wide doped lines and sintered in a fast firing process in a belt furnace. The silver contact fingers are centered on the doped lines. To account for the current flow through the base substrate, the evaluation follows the Eidelloth approximation [6]. A simulation-based correction also accounts for the local high-low junctions below the contacts. Details of this evaluation method will be published elsewhere [7].

3 RESULTS AND DISCUSSION

3.1 Influence of laser parameters on contact resistivities

Figure *2* shows measured specific contact resistivities as a function of the distances between pulse centers, for both the Gaussian beam profile and the flat-top profile.

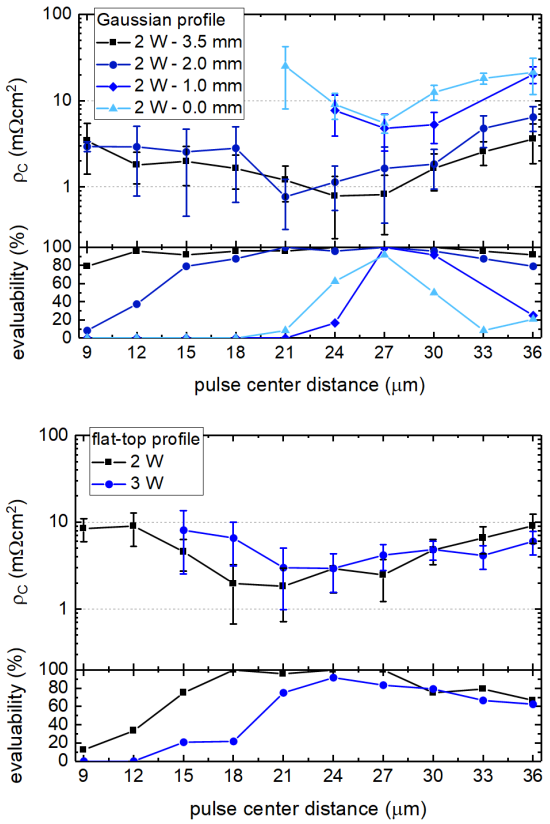

Figure 2: Specific contact resistivity plotted against laser pulse distance for a Gaussian laser profile with a variation of the laser focus (upper graph) and flat-top beam profile with a variation in laser power (lower graph).

With both beam profiles a minimum of the specific contact resistivity is reached at a pulse distance of 21-27 µm. Also, the evaluability of the TLM measurements, shown in the lower part of the graphs, has a maximum at the optimum pulse spacings. The evaluability indicates the percentage of measured structures whose linear fit of the TLM evaluation reaches an R^2 value greater than 0.99 and can thus be considered to be reliably and homogeneously contacted. Accordingly, higher contact resistances are obtained for very large and also for small pulse overlaps. For both Gaussian and flat-top laser pulse, the achieved contact resistivities tend to be lower for the lower fluences, i.e. lower power for flat top and larger defocus for Gaussian profiles. For the Gaussian beam profile, already a defocus of 2.0 mm leads to higher average contact resistances compared to a defocus of 3.5 mm and a reduced evaluability for low point distances. For 1.0 and 0.0 mm defocus this effect becomes so strong that up to 21 µm point spacing almost no measurement shows a linear correlation within the TLM evaluation and thus allows an evaluation. Likewise, the contact resistances for the larger pulse distances are significantly increased.

This already gives a hint that the surface damage induced by the laser pulses has an impact on the contactability of the laser-doped surfaces, because the resulting doping profiles do not fully account for the observed differences as will be shown in the next section.

3.2 Doping profiles

Figure *3* shows the doping profiles that are obtained using different laser parameters.

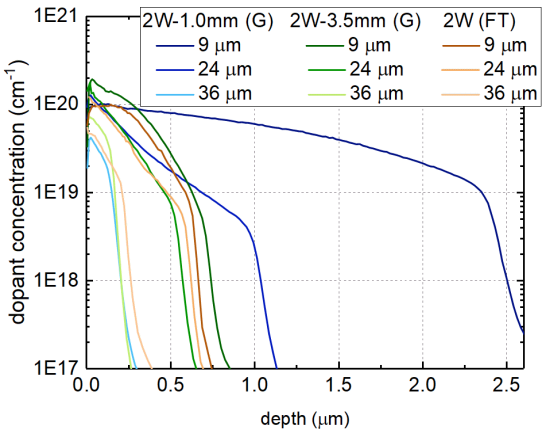

Figure 3: Doping profiles of laser doped samples with different laser parameters.

Green and blue lines indicate doping profiles generated by Gaussian laser pulses with 2 W and 1.0 or 3.5 mm defocus, respectively. In brown, doping profiles obtained at 2 W power with the flat top laser pulses are shown. For each set of laser parameters, the doping profile at 9, 24 & 36 µm pulse spacing is shown, in order to represent the minimum and maximum pulse spacing (9 and 36 µm), as well as the mostly optimal pulse spacing (24 µm) with respect to ρ_C. Indeed, the shallow doping profiles with a much lower surface concentration at 36 µm pulse spacing could explain the increase in contact resistivity at large pulse spacing. However, at 9 µm pulse spacing, profiles with similarly high surface concentrations of about 1×10^{20} cm^{-1} compared to those at 24 µm, are obtained. For the highly focused Gaussian laser pulses (1 mm defocus), a very deep doping profile is obtained at the small pulse spacing of 9 µm due to locally multiple melting events. Interestingly, according to Figure 2, no significant contact formation takes place with these

laser parameters and pulse spacings, indicating that the achieved doping levels play a minor role at low pulse spacings. Thus, we conclude that the different doping profiles cannot be the main reason for the shown dependence of the contact resistivity on the pulse spacing.

3.3 Kelvin probe force microscopy

To understand what happens on the silicon surface during laser doping, we perform KPFM imaging of laser-doped smooth FZ-Si samples. In this AFM mode the surface potential of a sample is measured locally and can therefore depict the local dopant concentration. Accordingly, the KPFM images depicted in Figure *4* show the local dopant concentration of the upper right edge of laser-doped lines with pulse spacing of 36 µm (a), 24 µm (b), and 9 µm (c), using the flat-top beam profile at 2 W. Especially in Figure *4*a the nearly square shapes of the areas doped by single laser pulses are clearly visible. Within their upper half there is an area of stronger contrast surrounded by artifacts indicating a heavily doped but also potentially damaged area created by excessive laser fluence. It is circled in green for more clarity. The brighter artifacts originate from surface structures and thus indicate the melting edge. In addition, elliptical secondary maxima can be seen next to the main spot. Comparing the images a-c with the specific contact resistances depicted in Figure *2*, it can be deduced that no significant contact formation occurs when these heavily melted areas of highest fluence overlap in such a way that they form a continuous surface.

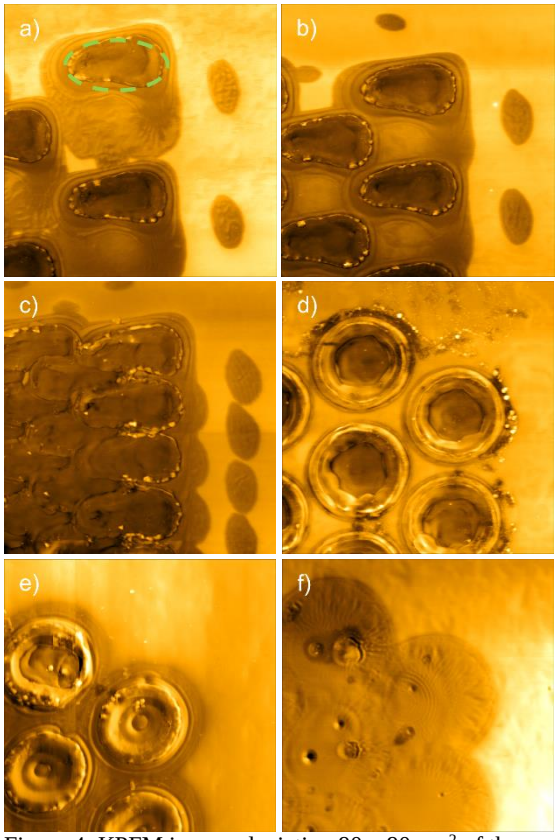

Figure 4: KPFM images depicting 90 x 90 µm^2 of the upper right edge of laser doped lines with point distances of 36, 24 & 9 µm (a-c) on a FZ-Si substrate created by the flat-top profile at 2 W and with a fix pulse distance at 36 µm, and 1, 2 & 3.5 mm (d-f) defocus created by the Gaussian profile.

If the pulse spacing is increased, areas with lower doping and less surface damage are formed between these strongly damaged areas, which allows for lower contact resistances (cf. Figure 2b). However, as the pulse spacing continues to increase, the contact resistivity rises again. This seems to be the case when the damaged but highly doped areas are no longer in contact. Therefore, multiple melting processes no longer occur in the regions of increased peak fluence and the obtained doping profiles start to show reduced surface concentrations.

Figure 4d-f instead shows laser doped sites created with the Gaussian profile at a constant pulse spacing of 36 µm but an increasing defocus of 1.0, 2.0 & 3.5 mm. Figure *4*f shows several laser spots with 3.5 mm defocus, forming an almost undamaged, uniformly doped surface with a dark KPFM contrast that corresponds to the low doping concentration shown in Figure *3* (bright green line). That same contrast can be found in Figure *4*e, surrounding melted and thus potentially damaged areas in the center of the laser doped spots produced with 2 mm defocus. These moderately doped areas are still forming a continuum in this case, whereas they vanish with 1 mm defocus as shown in Figure 4d, leaving only unconnected highly doped and highly damaged single spots. This phenomenon explains the similar behavior of ρ_C with respect to the pulse spacing at defocusing values of 2.0 and 3.5 mm, despite the significant difference in the laser damaged area. With a defocus of 1 mm and decreasing pulse spacing, only small areas of moderate doping are obtained, which would quickly disappear with increasing pulse overlap in favor of a fully damaged surface. This explains the drop in contactability between 21 and 24 µm pulse spacing in Figure 2.

3.4 Scanning electron microscopy

The conclusion that contacting takes place mainly in the areas between the damaged surfaces can be confirmed with the SEM images shown in Figure *5*. These images show the silicon surface after laser doping with flat top beam profile at 2 W, and subsequent screen-printing of a silver contact that has finally been removed with dilute HF. The area formerly covered with silver is on the right side of the image, whereas the left side shows the part of the laser-doped area that extended laterally beyond the silver finger. In this area the SEM images reveal the strong change of the surface structure in the heavily damaged areas by melting and recrystallisation, within the green circle in Figure *5*a. In the intermediate areas pyramid-like structures are found which show a small change in topology only at the pyramid tips. In Figure *5*b, at higher magnification, it can be seen that the pyramids are densely covered with silver crystallites in the lower half of the image, while almost no crystallites are found in the more damaged area in the upper half of the image.

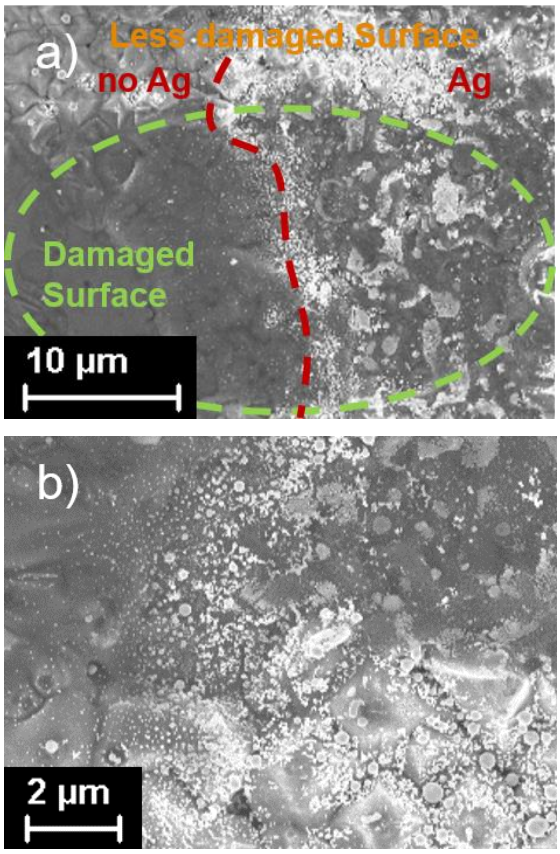

Figure 5: SEM images of a laser-doped area (flat-top) after removal of the screen-printed silver contact finger by HF. The area formerly covered by the silver finger is located right side of the image.

4 SUMMARY

In summary, high peak fluences during laser doping in particular lead to local damage and modification of the silicon surface, which in extreme cases can prevent the formation of silver crystallites during contacting by screen-printed silver paste. This occurs mainly at very small pulse spacing, which causes full-surface damage and thus prevents silver crystallite growth and contacting at all. Accordingly, an optimal combination of laser fluence and pulse spacing simultaneously provides a sufficiently high doping level and interconnected doped but undamaged areas between the pulse centers or other areas with higher damage due to excessive peak fluence, thus creating an environment in which silver crystallites can form.

5 ACKNOWLEDGEMENTS

Part of this work was supported by the German BMWK under contract 03EE1018B. The content of the publication is the responsibility of the authors.

REFERENCES

[1] International technology roadmap for photovoltaics, 14th edition, 2023
[2] M. Vaqueiro-Contreras et al., IEEE Journal of Photovoltaics 13(3) (2023) 373.
[3] M. Heilig et al., AIP Conference Proceedings 2147 (2019) 070004.
[4] K. Ohmer et al., IEEE Journal of Photovoltaics 1(2) (2011) 183.
[5] M. Kim et al., Solar Energy Materials and Solar Cells 132 (2015) 215.
[6] S. Eidelloth and R. Brendel, IEEE Electron Device Letters 35(1) (2014) 9.
[7] D. Wurmbrand, to be published